Nano Energy 30 (2016) 398–406

Contents lists available at ScienceDirect

Nano Energy

journal homepage: www.elsevier.com/locate/nanoen

Soft imprinted Ag nanowire hybrid electrodes on silicon heterojunction solar cells

Mark W. Knight[a], Jorik van de Groep[a], Paula C.P. Bronsveld[b], Wim C. Sinke[a,b], Albert Polman[a,*]

[a] Center for Nanophotonics, FOM Institute AMOLF, Science Park 104, 1098 XG Amsterdam, The Netherlands
[b] Energy Research Centre of the Netherlands (ECN), Westerduinweg 3, 1755 LE Petten, The Netherlands

ARTICLE INFO

Keywords:
Metal nanowires
Nanoimprint lithography
Nanofabrication
Anomalous transmission
Sheet resistance
Transparent electrode
Photovoltaics
Large area
Silicon heterojunction

ABSTRACT

We demonstrate enhanced efficiencies in front-contacted silicon heterojunction (SHJ) solar cells using silver nanowire-based hybrid electrodes. SHJ cells typically suffer from shading losses due to reflection from macroscopic sun-facing metal fingers, which must be closely spaced to avoid resistive losses in the transparent conductive electrode (TCE). Using substrate conformal imprint lithography (SCIL) we fabricate silver nanowire electrodes on practical scale (4.0 cm^2) planar SHJ cells. These electrodes exhibit anomalous transmission and a 7-fold improvement in sheet conductance relative to a standard ITO layer, enabling larger finger spacings and reducing reflection losses without compromising the cell fill factor. Over 70% of the ITO is replaced with transparent SiN_x, reducing the use of indium while improving the anti-reflective performance. Combined, the reduced shading and reflection raises the short circuit current density increases by 2.1 mA cm^{-2}, yielding an absolute increase in cell efficiency of 1.0%. These engineered hybrid electrodes provide a practical pathway towards front-contacted SHJ cells with a reduced dependence on rare metals and high efficiencies.

1. Introduction

Transparent conductive electrodes (TCEs), which ideally offer simultaneously high broadband transmission and low electrical resistance, are a key element in many optoelectronic devices [1] including display panels, organic light-emitting diodes, and solar cells. Currently, most devices rely on indium tin oxide (ITO) as a transparent conductor. However, after decades of optimization ITO has reached fundamental limits which specify an inherent tradeoff between optical and electrical performance [2,3]. Combined with expensive and unpredictable indium supplies [4,5] and fragility [6], there is a significant effort underway to develop next-generation electrodes with improved transparency and conductivity [7]. Numerous alternatives have been suggested [4,5], with metal nanowire networks among the leading candidates due to the high conductivity of metal. Initial demonstrations have been performed using a variety of fabrication methods, including chemical synthesis [8–14], electrospinning [11,15,16], lithographic patterning [17,18] and, more recently, nanoimprinting networks [19–21]. While these approaches have shown promise, the controlled fabrication of nanostructured electrodes over large areas with the size of practical solar cells has so far proved elusive.

The need for improved TCEs is particularly acute for solar cells based on a silicon heterojunction (SHJ), where a crystalline Si absorber is passivated by thin amorphous Si layers (Fig. 1a). These solar cells have attracted significant interest due to their record-setting voltage and efficiency [22–25], environmentally friendly processing, and ease of fabrication [23,26]. However, poor lateral conductivity in the doped a-Si:H layer requires the addition of a TCE to transport the high current produced by these cells without large losses. Typically ITO, this thin layer is optimized in thickness to act as a single-layer anti-reflection coating (ARC, ~80 nm). This thickness constraint results in limited conductivity, which then necessitates additional macroscopic metal 'fingers' to harvest the photogenerated electrons. Due to their width (typically > 80 μm), these fingers reflect sunlight, shading portions of the solar cell and causing a significant reduction in both current and cell efficiency [27,28]. The maximum allowed spacing between these fingers is strongly influenced by the resistance of the TCE [29,30], forging a direct relationship between TCE performance and cell efficiency.

Here, we demonstrate a large-area nanostructured hybrid TCE comprised of encapsulated Ag nanowires, which significantly exceeds ITO in conductivity with equivalent transparency, and replaces the monolithic ITO layer on a front-contacted and industrially-processed SHJ cell (Fig. 1a-d). This approach decouples, to a large extent, the optical and electrical properties of a TCE and enables the independent optimization of each functionality. In the new design, conduction in the

* Corresponding author.
E-mail address: polman@amolf.nl (A. Polman).

http://dx.doi.org/10.1016/j.nanoen.2016.10.011
Received 19 February 2016; Received in revised form 26 July 2016; Accepted 6 October 2016
Available online 13 October 2016

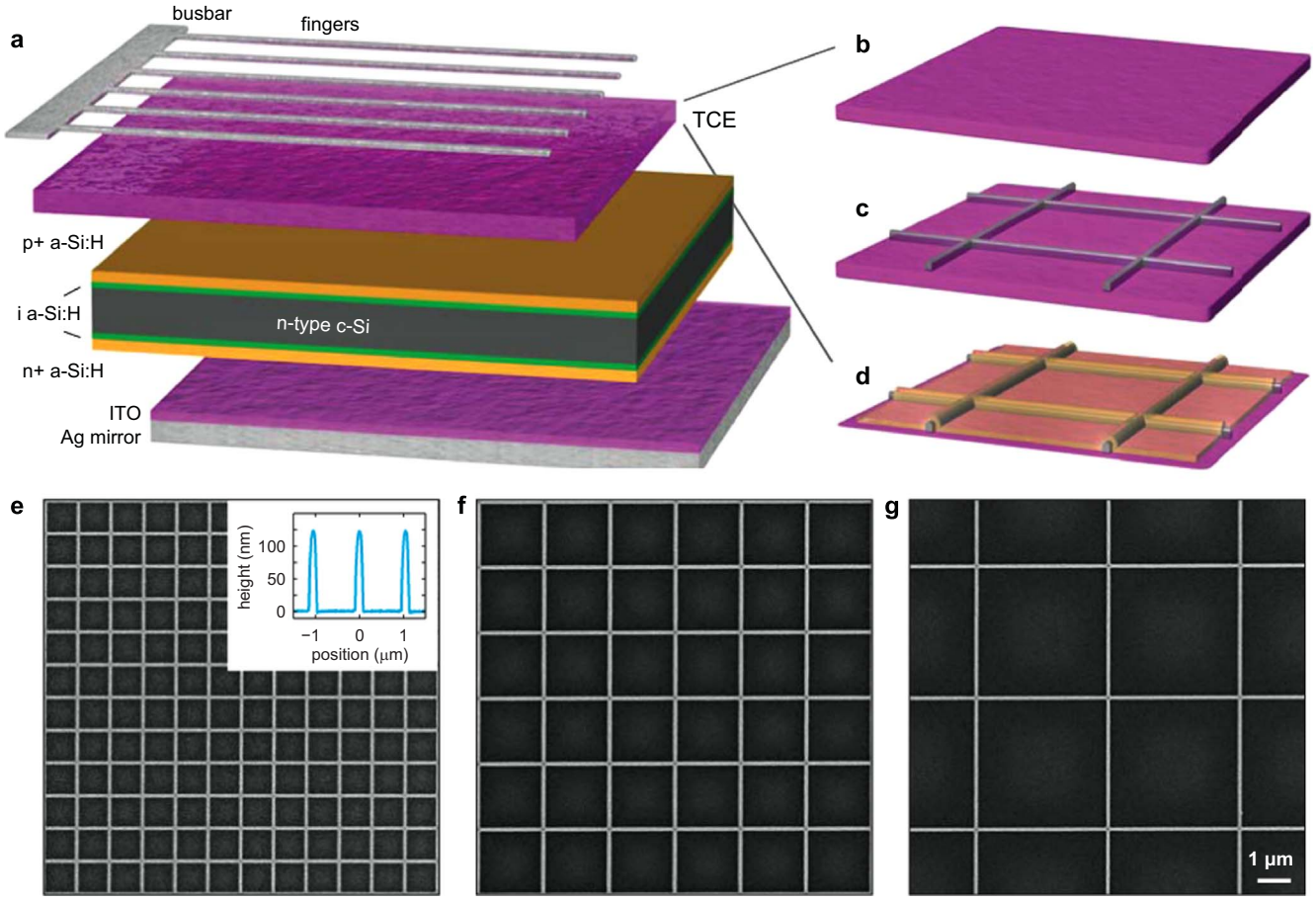

Fig. 1. Front-contacted planar silicon heterojunction (SHJ) solar cells. a, Schematic illustration of the HIT cells used in this work. **b,** The standard transparent conductive electrode (TCE) for SHJ cells, fabricated using 80 nm of indium-tin oxide (ITO) to serve as an ARC. **c,** ITO electrode/ARC modified with a conductive Ag nanowire (NW) grid. **d,** Hybrid electrode comprised of 22 nm of ITO for micron-scale conduction, a NW grid for cm-scale conduction, and an encapsulating SiN_x ARC (62 nm). **e-f,** Scanning electron micrographs showing representative areas of fabricated NW grids with pitches of 1, 2, and 4 μm. *Inset*: AFM cross section of 1 μm pitch NWs. The shared scale bar for all images is 1 μm.

electrode is primarily provided by the nanowire network, which is fabricated on an ultrathin ITO layer to provide controlled charge transport within the μm-scale interstitial regions. Plasmonic anomalous optical transmission, where the optical transmission is larger than expected considering the geometrical areas shaded/covered by the Ag-NW network, enables broadband transparency [18,31]. Separately, the single layer anti-reflection minimum is specified by a thin coating of silicon nitride that also serves as a protective encapsulant for the Ag nanowires (Fig. 1c-d). We apply this hybrid electrode to 4.0 cm^2 planar heterojunction solar cells, and demonstrate an absolute efficiency enhancement of 1.0% relative to reference cells with a standard 80 nm ITO layer and 2 mm finger spacing.

2. Results and discussion

2.1. Solar cell and hybrid electrode fabrication

The layout of the SHJ cells studied in this work are shown schematically in Fig. 1a. Briefly, a crystalline Si wafer (grey) is bifacially passivated with thin (~5 nm) intrinsic a-Si:H layers (green), with the front-surface heterojunction and the back-surface field formed using highly doped a-Si:H layers (orange). The cell is contacted on the front with a TCE (ITO, nanowire-enhanced ITO, or a nanowire hybrid (Fig. 1b-d)) and macroscale metallization, and on the rear with a conductive mirror.

Cell fabrication was conducted in two steps: the production of 5.5×5.5 cm^2 SHJ semicells, followed by deposition of a TCE (see Methods: nanowire network fabrication on SHJ semicells). The semicells, which were pre-metallization SHJ cells with either 80 nm or 22 nm of ITO on the front surface, were prepared using industrial equipment and processing techniques. Next, three nanowire network designs with different pitches (1, 2, and 4 μm, each covering 2.0×2.0 cm^2) were patterned into a sol-gel/PMMA bilayer using substrate-conformal imprint lithography (SCIL), which is a fast, high resolution, and dust-tolerant nanoimprint technique based on a soft polymer stamp [32,33]. After the SCIL imprint, a subsequent evaporation and liftoff produced complete Ag nanowire networks with a geometry dictated by the stamp. For the semicells with the thin (22 nm) ITO layer, the hybrid electrode was completed via encapsulation of the nanowires within a 62 nm layer of SiN_x to protect against oxidation and serve as a single layer ARC. After completion, the four cell designs (three nanowire-based cells and a wire-free reference) were laser-cut into 2.5×2.5 cm^2 cells, leaving sufficient space around the nanowire networks to enable a masked measurement without the influence of edge recombination [34].

The completed Ag nanowire grids (2.0×2.0 cm^2) were free of visible defects, and exhibited uniform nanowire dimensions across all networks. Representative SEM images of networks with pitches of 1, 2, and 4 μm are shown in Fig. 1e-f, respectively, with wire widths on all samples measured to be 80 ± 5 nm. An AFM cross section of the networks shows a wire height of 120 nm (Fig. 1e, inset).

2.2. Network conductivity

To directly measure their electrical sheet resistance, nanowire networks identical to those on the SHJ cells were fabricated on

Table 1
Measured sheet resistances for the ITO and NW electrodes. For the NW electrodes, the sheet resistances calculated from the measured dimensions and conductivity of bulk Ag are listed in parentheses. These measured resistances are plotted against modeled transmission through the electrode in Fig. S1, where both absorption and reflection contribute to the reduction in transmission.

Conductive layer	Sheet resistance (Ω/sq)
ITO (80 nm)	110 ± 10
ITO (22 nm)	260 ± 10
NW grid (1 μm pitch)	4.0 *(1.6)*
NW grid (2 μm pitch)	7.2 *(3.3)*
NW grid (4 μm pitch)	15.0 *(6.6)*

nonconductive glass substrates. For the ITO, films were simultaneously deposited on reference SHJ cells where the depletion region formed an insulating barrier, enabling measurement of only the ITO sheet resistance. Both the nanowire networks and ITO films were characterized using 4-point probe measurements (see Methods: electrical characterization).

The measured sheet resistances are listed in Table 1, with the nanowire networks showing an order of magnitude improvement relative to the standard ITO film. The 80 nm ITO layer measured 110 Ω/sq, a sheet resistance resulting from the combined effects of the ARC thickness constraint, fundamental constraints (transparency requires relatively low free carrier densities) [2,5], and carrier mobility limitations resulting from the industrial sputtering method. This sheet resistance is quite close to an optimized sheet resistance of 100 Ω/sq; while higher conductivity ITO may be fabricated, in the range of 40–80 Ω/sq, the increased conduction does not compensate for the current lost due to parasitic absorption [3]. The thin ITO layer (22 nm) showed an increased sheet resistance of 260 Ω/sq, a lesser increase than the four-fold increase expected from reducing the thickness of a uniform film. This suggests the sputtering process used for film deposition results in depth- or thickness-dependent ITO properties.

In stark contrast to the relatively high sheet resistance of the reference ITO, the nanowire networks measured only 4.0, 7.2, and 15.0 Ω/sq for 1, 2, and 4 μm pitched networks, respectively (Table 1). The measured doubling of sheet resistance with pitch is expected from the analytical description of resistance in a large 2D network of nanowires: $R_S=\rho L/A$, where ρ is the conductivity, L is the network pitch, and A is the cross sectional area of the wire [19]. Using the measured nanowire dimensions for A, assuming the bulk value of ρ_{Ag}, and neglecting interfacial effects this model gives R_s of 1.6, 3.3, and 6.6 Ω/sq for the experimental pitches (Table 1, in parentheses). From these, we calculate an effective resistivity of only $\rho_{eff}\approx 2.3\times\rho_{Ag}$, which is a marked improvement over the previously reported value of ~5.7 for lithographically defined networks [18] and results from improved metallization conditions which produce larger crystalline grains. The remaining difference between ρ_{eff} and ρ_{Ag} is attributed to grain boundary and surface scattering [35], *in situ* oxidation during deposition, and the formation of a thin environmental surface oxide that reduces the volume of conductive metal.

The high degree of uniformity of these networks ensures that charge carriers will experience the 'local' sheet resistance of the thin residual ITO layer within the interstitial regions of the networks (1–4 μm), and then the reduced 'global' sheet resistance of the nanowire network over longer distances. This uniformity is a key advantage of nanofabrication, which can create networks with a degree of local optimization (μm to cm-scale) and uniformity unachievable through chemical synthesis or electrospinning.

2.3. Solar cells with nanowires on 80 nm thick ITO

First, we show that a more conductive TCE permits an increase in finger pitch, leading to an increase in J_{sc} without a corresponding

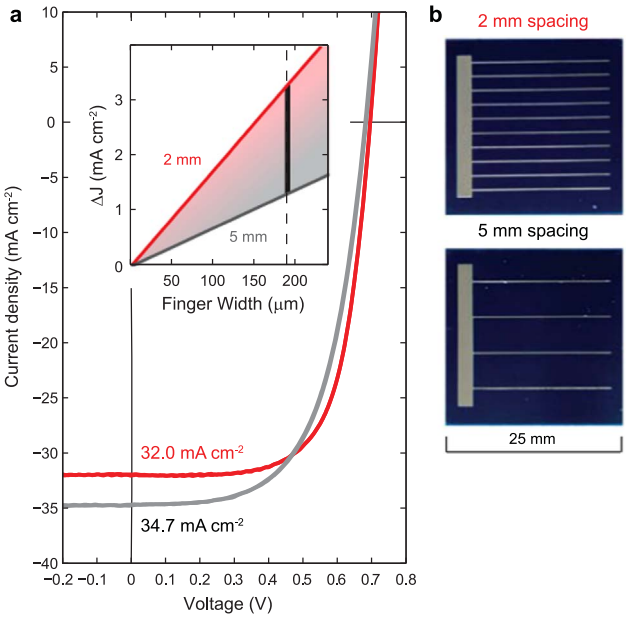

Fig. 2. Optical shading from fingers. a, Current-voltage response of flat SHJ cells with an 80 nm layer of ITO (110 Ω/sq) showing the reduction in shading losses as the finger spacing is increased from 2 mm (red) to 5 mm (grey). *Inset*: geometrical loss of J_{sc} due to finger shading, based on a local current density of 36.0 mA cm^{-2}; the vertical black line corresponds to the experimental finger width. **b,** Photographs of fabricated cells with 2 mm and 5 mm finger spacings. (For interpretation of the references to color in this figure legend, the reader is referred to the web version of this article.)

reduction in *FF*. This increased conductivity is achieved by applying nanowire networks to flat SHJ cells with a standard 80 nm ITO layer. We will then show, in a second geometry, how Ag nanowires enable a reduction of the ITO layer thickness.

For the flat reference cells, with 80 nm ITO as the TCE, the influence of finger spacing on J_{sc} is clearly visible in the IV response (Fig. 2). With the industry-standard finger spacing (2 mm, red line), J_{sc}=32.0 mA cm^{-2}. By increasing the finger spacing to 5 mm, J_{sc} increases by 2.7 mA cm^{-2} to 34.7 mA cm^{-2} (grey line). This difference is the direct result of geometric shading, which gives a reduced current

$$J'_{sc} = J_{sc}\,(1 - t\,A), \tag{1}$$

where A is the fractional area covered by metal, and t is an correction factor to account for transmission through fingers. For opaque, macroscopic fingers t is unity. The magnitude of the shading loss ($\Delta J=J_{sc}-J_{sc}'$) depends on finger width and is plotted in Fig. 2a (inset). The potential improvement in current from an increased finger pitch is indicated by the shaded region and, for typical finger widths, can range from 0.5 to 2.2 mA cm^{-2}. For our measured finger width of 185 μm, ΔJ=2.0 mA cm^{-2}, in agreement with the observed difference in short circuit current combined with resistive losses.

However, this increase in current comes at the expense of lost fill factor (*FF*:0.676 reduced to 0.604) due to increased series resistance. Given a uniform carrier generation profile, increased finger spacing causes a linear increase in current transported through the ITO, increasing J^2R_{sh} losses and decreasing *FF*. Since cell efficiency $\eta = FFV_{oc}J_{sc}/P_{in}$, the gains in J_{sc} are countered by the reduction in *FF*. This effect is well known: the optimal finger pitch is determined by J_{sc}, which depends on finger width and, crucially, the TCE sheet resistance (R_{sh}) [29]. By adding nanowires, which can achieve low values of R_{sh} relative to ITO (Table 1), we can increase this optimal finger spacing from 2 mm to 5 mm (Fig. S2).

However, adding Ag nanowires without modifying the ITO thickness can introduce additional parasitic optical loss at the cell surface. To understand the optical impact of the nanowires on cell efficiency, the absorption of light in the nanowire-modified cells (which includes

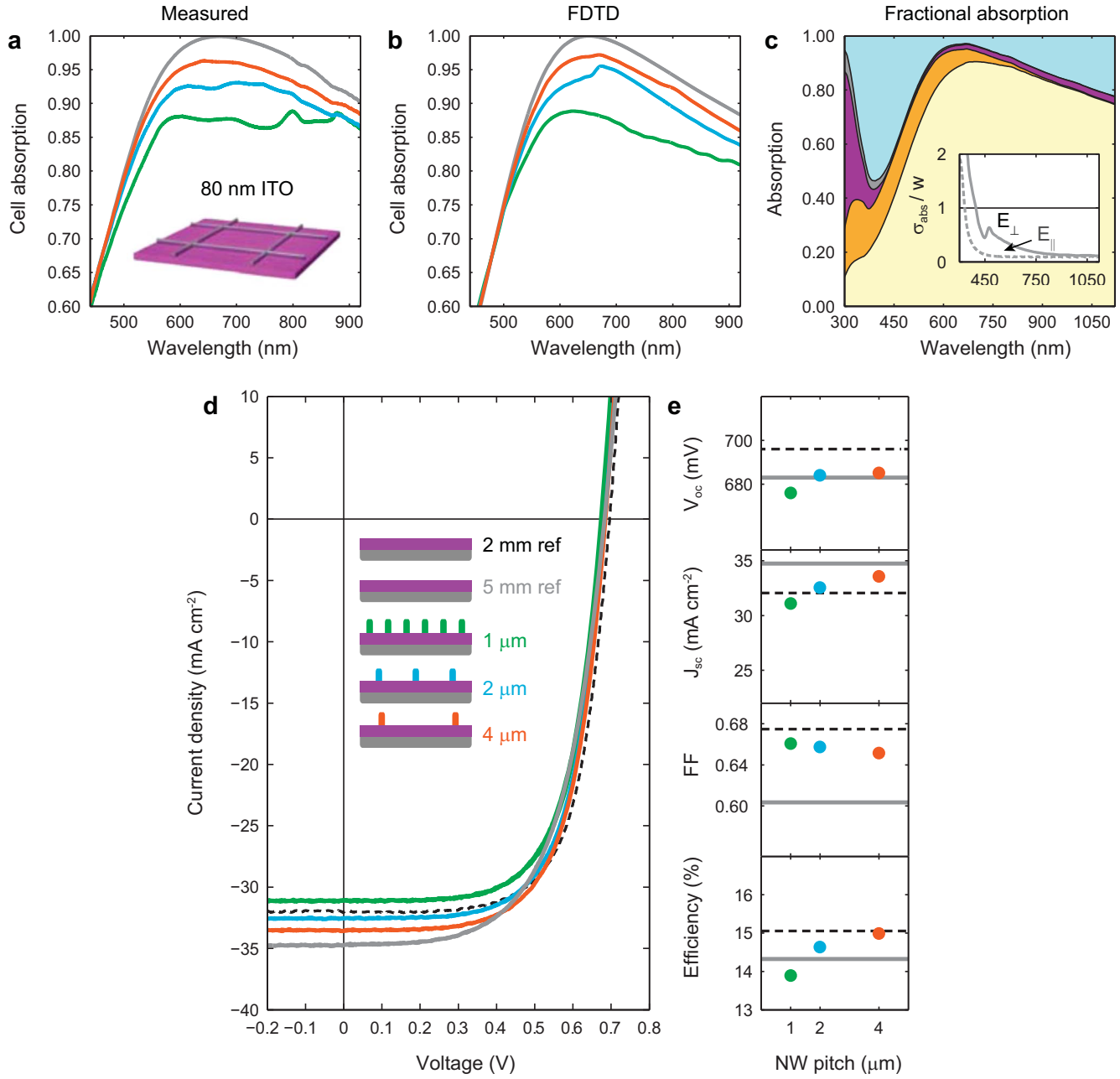

Fig. 3. Optical and electrical properties of planar SHJ cells with 80 nm ITO and Ag nanowire grids. a,b, Measured and simulated spectra for nanowire grids with pitches of 1 μm (green), 2 μm (blue) and 4 μm (orange) fabricated on SHJ cells with standard-thickness ITO (80 nm). The reference cell has only ITO and no nanowires (grey). **c,** Modeled fractional absorption for a NW network on 80 nm ITO with a 4 μm pitch, with shaded areas indicating useful absorption in the Si (yellow), parasitic absorption in the amorphous Si:H (orange), parasitic absorption in the ITO (purple), and parasitic absorption in the nanowires (dark grey). The remaining area indicates reflection (blue). *Inset*: absorption efficiency of an isolated nanowire on a SHJ cell, calculated for polarization parallel ($E_{||}$) and perpendicular ($E_\perp$) to the nanowire axis. **d,** Measured IV response and **e,** Summarized cell parameters for SHJ cells with a 5 mm finger spacing and ITO covered with Ag NW networks. Values for the standard reference cell (2 mm finger pitch, 80 nm ITO) are indicated by the dashed black lines. (For interpretation of the references to color in this figure legend, the reader is referred to the web version of this article.)

both carrier generation in the c-Si and parasitic absorption in the other layers) was determined by measuring reflection spectra in the interstitial regions between fingers (see Section 3.2). These measurements were correlated with a 3D finite-difference time-domain (FDTD) model using measured dimensions for the nanowires and thin film layers (ITO and a-Si:H) as well as measured optical constants.

The experimental and modeled cell absorption spectra show the dependence of plasmonic scattering and absorption losses on nanowire pitch (Fig. 3a,b). Without nanowires, the cells show perfect absorption when the $\lambda/4n_{ITO}$ anti-reflection condition in the ITO ARC is met (λ=670 nm), while reduced absorption is observed at shorter and longer wavelengths. The addition of nanowires introduces additional scattering losses and causes the overall cell absorption to decrease. However, for the largest network pitch (4 μm), this scattering loss is only ~4% at the anti-reflection peak. The agreement between the measured spectra and the FDTD model is remarkable given that the measurement compares a measured area of ~4 mm^2 (~10^6 nanowires) to a single idealized unit cell.

In addition to scattering losses, the model enables us to identify which cell layers are responsible for parasitic absorption (Fig. 3c). While most of the light is converted to charge carriers within the crystalline Si (light yellow shaded area), there is significant parasitic absorption in the doped a-Si:H layer (orange) and the ITO (purple), a problem common to all front-contacted SHJ cells. For ITO, this

absorption is due to direct interband transitions above the ITO bandgap (E_{gap}~4.0 eV), with loss extending from the UV into the blue due to logarithmically decreasing absorption commonly referred to as an 'Urbach tail' [2,36]. For lower energies, near the Si bandgap (E_{gap}=1.1 eV), ITO suffers from free carrier absorption. Integrated over the AM1.5 G spectrum, these effects cause a current density reduction of 0.93 mA cm^{-2}. By contrast, the Ag nanowire network has very low absorption, with only 0.24 mA cm^{-2} lost (small grey region). Since the Rayleigh anomaly for these grids occurs outside of the Si absorption window [18], and higher-order diffraction is usually weak, the nanowire-related absorption can be understood from the absorption of individual nanowires (Fig. 3c, *inset*). For light polarized parallel to the nanowire, translational symmetry prevents plasmonic excitation and only UV interband transitions contribute to the absorption. For transverse polarization, a weak dipolar plasmonic oscillation can be excited. For both polarizations the geometrically-tuned optical absorption cross section is less than the physical cross section, which gives rise to anomalously high transmission.

The modified cells exhibit an IV response that depends strongly on nanowire pitch, with both *FF* and J_{sc} affected (Fig. 3d,e). Crucially, the nanowire fabrication process preserves high quality cell passivation as evidenced by the consistent values of V_{oc} for cells with and without nanowires (Table 2).

Increased nanowire pitches show corresponding increases in J_{sc} (Fig. 3d,e), in agreement with the cell absorption spectra in Fig. 3a. For the largest pitch (4 μm) J_{sc}=33.6 mA cm^{-2}, which is a current reduction of only 1.1 mA cm^{-2} relative to the wire-free (and low *FF*) reference cell. Our optical model accurately reproduces this difference in J_{sc}, predicting 1.0 mA cm^{-2} of parasitic plasmonic loss (Table 2). Interestingly, this corresponds to an effective shaded area of only 0.62 A_w (where A_w is the area fraction of the cell covered by nanowires), and highlights a key advantage of nanoscale metallization: spectrally narrow resonances can be detuned from the solar spectrum, allowing anomalous transmission corresponding to t=0.62 in Eq. (1). This low optical loss relative to ITO, combined with reduced shading from the increased finger spacing, yields a net increase of 1.6 mA cm^{-2} (33.6 *vs.* 32.0 mA cm^{-2}) relative to the 'standard' cell geometry (2 mm finger spacing, 80 nm ITO).

In addition to increased current, the 4 μm-pitched nanowire cell shows an increase in *FF* relative to the ITO-only cell with 5-mm spaced fingers 0.604–0.652). This *FF* increase is the result of reduced series resistance, because the 110 Ω/sq ITO layer is supplemented by the low resistance (15 Ω/sq) NW network. Importantly, these gains could not be realized using a thicker ITO layer since this would both result in a non-optimal ARC and increased parasitic loss from free carrier and interband absorption.

For the 5 mm fingers, the result of the simultaneously increased J_{sc} and *FF* is an increase in efficiency from the *in situ* 14.3% reference to 15.0%. Compared to the 2 mm-spaced cell, however, no net efficiency increase is measured (15.0% *vs.* 15.0%). This is likely because the reference with 2 mm-spaced fingers was fabricated on a separate wafer with lower bulk recombination, giving the reference a slightly higher V_{oc} and *FF*, and cancelling the nanowire cell's current gains. Furthermore, this nanowire-enhanced cell geometry does not yet reduce the use of indium, and, prior to encapsulation in a module, has the potential for Ag oxidation losses due to environmental exposure.

Table 2
Summary of the current-voltage (IV) properties for the Ag-NW integrated SHJ cells. J_{sc} values in parenthesis correspond to modeled current generation in the Si substrate, corrected for the geometric shading loss from 185 μm fingers.

Wafer	ITO (nm)	Finger spacing (mm)	NW pitch (μm)	V_{oc} (mV)	J_{sc} (mA cm^{-2})	*FF*	*Eff.* (%)
Wafer 1 *standard ref.*	80 nm	2.0	–	696	32.0 *(33.1)*	0.676	15.0
Wafer 2 a	80 nm	5.0	–	683	34.7 *(33.5)*	0.604	14.3
Wafer 2 b	80 nm	5.0	1.0	676	31.1 *(29.9)*	0.661	13.9
Wafer 2c	80 nm	5.0	2.0	684	32.5 *(31.6)*	0.657	14.6
Wafer 2 d	80 nm	5.0	4.0	685	33.6 *(32.5)*	0.652	15.0
Wafer 3 a	22 nm	5.0	–	696	34.9 *(35.1)*	0.610	14.8
Wafer 3 b	22 nm	5.0	1.0	699	30.1 *(30.5)*	0.673	14.2
Wafer 3c	22 nm	5.0	2.0	699	32.5 *(32.6)*	0.665	15.1
Wafer 3 d	22 nm	5.0	4.0	701	34.1 *(33.8)*	0.670	16.0

2.4. Hybrid electrodes on solar cells

Both of these issues are resolved by a hybrid electrode design consisting of Ag NWs on a very thin (22 nm) ITO layer that are encapsulated by SiN_x (62 nm). This design results in a 4-fold reduction of the amount of indium required to produce a cell, while retaining conductivity in the interstitial regions and, due to the conformal SiN_x overlayer, is stabilized against environmental oxidation and sulfurization [37–40]. The residual ITO thickness must be above ~10 nm for three reasons: (1) to protect the passivating a-Si:H during the nanowire fabrication, (2) to minimize parasitic absorption in the a-Si layers by spatially reducing overlap of the concentrated plasmonic near-fields with the high index a-Si layers ($n_{a\text{-}Si}$=3.6–4.4 from 1.12–3.0 eV), and (3) to minimize the substrate-induced redshift and achieve spectral separation between the plasmonic NW resonances and the solar spectrum maximum [41]. This approach is distinct from prior random electrodes where the TCO doubles as the AR layer [14], allowing the AR layer thickness to be optimized independently from the TCE conductivity and achieving nearly complete elimination of parasitic optical losses from the ITO. These hybrid electrodes were fabricated similarly to the networks on 80 nm thick ITO, then overcoated with low temperature PECVD SiN_x (see Methods: nanowire network fabrication on SHJ semicells).

Optically, the hybrid electrode results in both lower parasitic absorption and lower cell reflection relative to equivalent Ag networks on 80 nm ITO. The reduced reflection can be clearly seen in the measured and modeled cell absorption spectra (Fig. 4a-c). For the most transparent network (4 μm pitch) the additional scattering loss is only ~3% at the anti-reflection peak, with reduced loss in the red spectral range relative to the ITO-only case (Fig. 3a,b). This is due to the fact that the SiN_x has a refractive index which is nearly constant above the Si bandgap and is well suited for a single-layer ARC (n_{SiNx}=2.0–2.07 from 1.12–3.0 eV), while that of ITO is strongly dispersive with energy. The reduction in absorption is less intuitive since the addition of a dielectric shell around the plasmonic nanowires induces a redshift of the transverse localized surface plasmon resonance into the visible, causing an increase in fractional absorption (Fig. 4c, grey region: 0.55 mA cm^{-2}, compared to 0.24 mA cm^{-2} in Fig. 3c). This slight increase in nanowire absorption is countered by the nearly complete elimination of parasitic ITO loss (purple region: decreases from 0.93 to 0.24 mA cm^{-2} compared to Fig. 3c). In our experimental measurements, the reduced absorption combines with the improved anti-reflection properties to produce a net gain in measured J_{sc} of 0.5 mA cm^{-2} relative to the nanowire-enhanced ITO case (Table 2).

Interestingly, the small amount of nanowire absorption indicates that encapsulated networks retain the property of anomalous transmission (t=0.77 in Eq. (1)). This is because, while the nanowires function as lossy nanoscale antennas in a narrow spectral regime and for

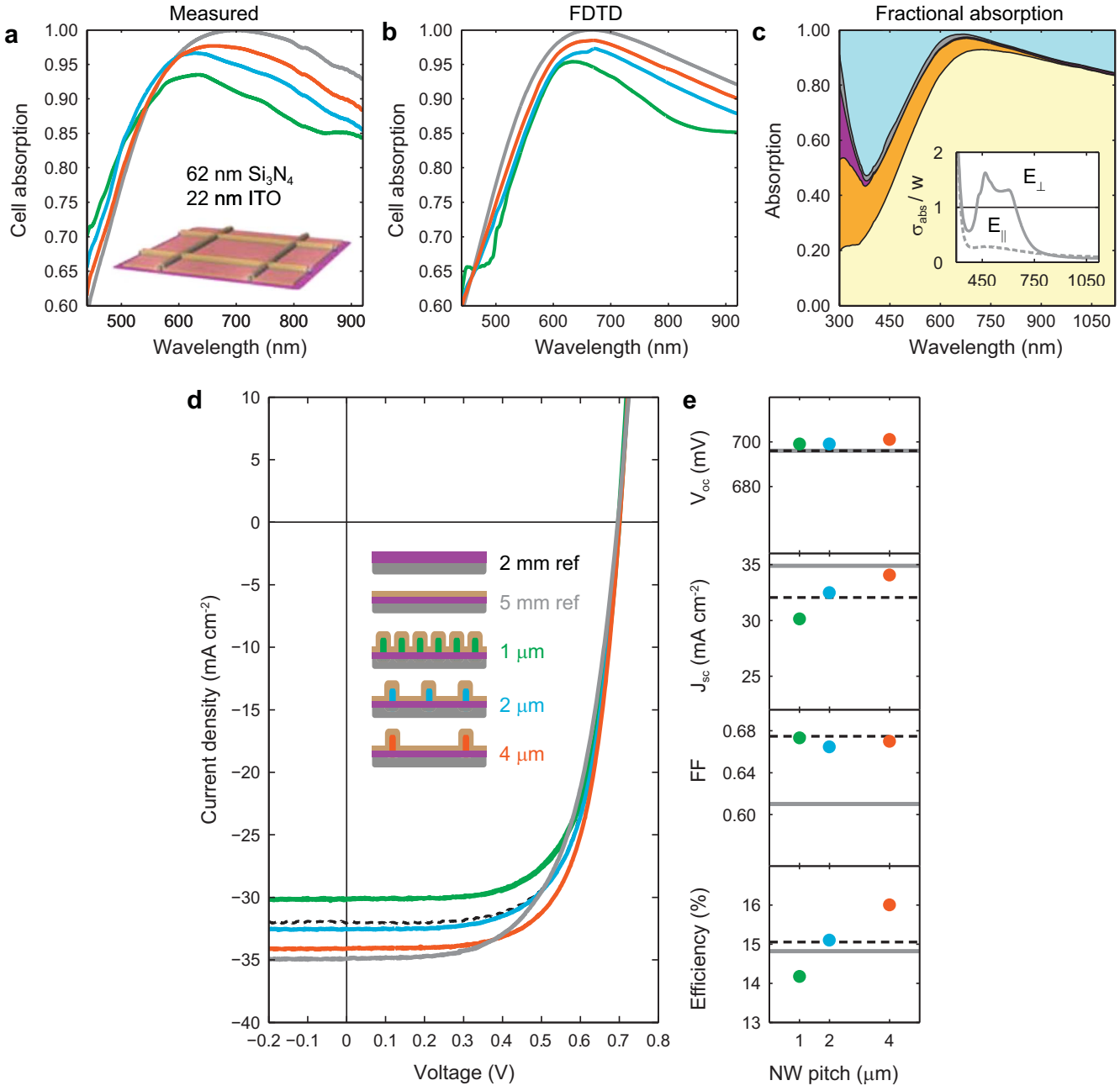

Fig. 4. Optical and electrical properties of planar SHJ cells with Ag nanowire hybrid electrodes. a-b, Measured and calculated cell absorption spectra for nanowire grids with periods of 1 μm (green), 2 μm (blue) and 4 μm (orange) fabricated on SHJ cells with a thin ITO layer (22 nm), and a 62 nm SiN_x overcoat. The reference cell (grey) has only the ITO/SiN_x layers. **c,** Modeled fractional absorption for the best performing hybrid SHJ cell (4 μm NW pitch), showing useful absorption in the Si (yellow), parasitic absorption in the amorphous Si:H (orange), parasitic absorption in the ITO (purple), and parasitic absorption in the nanowires (dark grey). The remaining area indicates reflection (blue). *Inset*: absorption efficiency of an isolated nanowire on a SHJ cell, calculated for polarization parallel ($E_{||}$) and perpendicular ($E_{\perp}$) to the nanowire axis. **d,** Measured IV response and **e,** Summarized cell parameters for planar SHJ cells with a 5 mm finger spacing and NW hybrid electrodes. Values for the standard reference cell (2 mm finger pitch, 80 nm ITO) are indicated by the dashed black lines. (For interpretation of the references to color in this figure legend, the reader is referred to the web version of this article.)

transverse polarization, most of the broadband solar photons remain detuned and the AM1.5 G averaged value of σ_{abs} remains below unity (Fig. 4c, inset). As with the nanowires on 80 nm ITO, symmetry forbids plasmonic excitation for light polarized parallel to a nanowire and absorption is limited to UV interband transitions. This antenna-based anomalous transmission is unique to nanoscale 'fingers,' where the physical and optical cross sections can diverge as a result of resonant behavior.

SHJ cells with hybrid electrodes show enhanced efficiencies relative to those with thick ITO due to a simultaneous increase in FF and J_{sc} (Fig. 4d). For a reference cell with thin ITO (260 Ω/sq), series resistance causes significant J^2R losses and a correspondingly low *FF* (0.610). For all nanowire pitches, the sheet resistance is sufficiently low (≤15 Ω/sq) to achieve the maximum *FF* for these semicells (Table 2: 0.670 ± 0.01). The lack of a *FF* falloff for increasing pitch indicates that 5 mm does not exceed the optimal finger spacing, in agreement with finger spacing optimization shown in Fig. S2. As with the thicker ITO layer, adding nanowires does not affect V_{oc}, indicating that passivation is unaffected by the SCIL fabrication process even on a thin ITO layer. With nearly constant values of *FF* and V_{oc}, the efficiency of the hybrid electrode SHJ cells is directly proportional to J_{sc}, which is determined by the transparency of the top electrode. As shown in the optical spectra (Fig. 4a-b), increased nanowire pitch corresponds to increased transparency.

For the largest pitch (4 μm), the measured J_{sc} exceeds the current of the 80 nm ITO reference cell by 2.1 mA cm^{-2}, which is the result of reduced shading from increased finger spacing and low optical loss from the nanowires. Based on the local integrated EQE spectra (Fig. S3), we have analyzed the range of finger widths where cells would benefit from this nanowire electrode (Fig. S4). Our measured hybrid networks, which introduce a 3% local optical loss relative to 80 nm ITO, can improve the efficiency of cells with fingers wider than 80–100 μm.

This current increase, combined with *FF* and V_{oc} equal to the standard reference device, gives a 16.0% efficient cell. This is an improvement in absolute efficiency of 1.0% relative to the 80 nm ITO reference cell using a standard 2 mm finger spacing. Even with a fully optimized finger spacing, based on the experimental finger width and sheet resistance, the reference cell could achieve only 15.3% efficiency (Fig. S2), falling short of the nanowire-enhanced cell efficiency.

3. Conclusions

We have demonstrated silver NW-based transparent electrodes that enhance the power efficiency of practical-scale planar SHJ solar cells. These electrodes exhibit anomalous transmission and a 7-fold improvement in sheet conductance relative to an 80 nm reference ITO layer, enabling an increase in finger spacing from 2 to 5 mm without loss of *FF*. We show two geometries: silver NW-enhanced ITO, and a silver NW/SiN_x hybrid electrode. For the NW-enhanced ITO, the high conductivity enables an increase in macroscopic finger spacing, increasing J_{sc} by 1.6 mA cm^{-2} without compromising the *FF*. The hybrid electrode, in addition to high conductivity, achieves improved ARC performance in the interstitial regions of the NW network by replacing > 70% of the ITO with SiN_x. Due to the low dispersion of SiN_x, and elimination of parasitic absorption from the ITO, the improvement in J_{sc} rises to 2.1 mA cm^{-2}. As a result, these planar SHJ cells modified with hybrid electrodes show an enhancement in power conversion efficiency from 15.0–16.0%. This increase is partially due to the use of industrially prepared ITO with a sheet resistance of ~110 Ω/sq. Improvements in ITO quality, along with the application of narrower fingers than are currently screen-printed, would reduce this relative improvement.

While shown here for untextured cells, to clearly elucidate the underlying physics, the fabrication enabling this hybrid TCE is fully compatible with micro- and nano-photonic texturing, including Mie resonators [42] and inverted micropyramids [43]. With texturing to address optical reflection, these hybrid electrodes provide a practical pathway towards front-contacted SHJ cells with high efficiencies and with a reduced dependence on rare metals.

4. Methods

4.1. Nanowire network fabrication on SHJ semicells

Flat, monofacial silicon heterojunction semicells were prepared on 5.5×5.5 cm^2 float zone Si wafers (280 ± 10 μm thick, n-type, < 111 >, 1–5 Ω-cm) with either 22 nm or 80 nm of sputtered ITO on the sun-facing surface. First, the wafers were bifacially passivated with a thin (5 nm) layer of intrinsic a-Si:H, giving millisecond carrier lifetimes (2–10 ms). Thin, highly doped a-Si:H layers were then deposited to form the a-Si/c-Si heterojunction and a back surface field. The rear of the cell was contacted with a conductive mirror (ITO+Ag), and the sun-facing surface of the semicell was sputtered with ITO. All semicell processing steps were performed at the Energy Research Center of the Netherlands (ECN) using equipment and methods compatible with industrial scale production.

To create the nanowire pattern the semicells were first cleaned by 5 min sonication in H_2O, dried with N_2, and then annealed under vacuum for 30 min at 180 °C to repair damage from the ITO sputtering [44]. Next, ~500 nm PMMA 35k(500) was spincoated at 1000 rpm for 45 s, followed by a 5 min bake at 150 °C. To make the PMMA surface hydrophilic a short O_2 reactive-ion etch (RIE) was performed (descum: 10 s, 5 mTorr, 50 W, with 25 sccm O_2). Liquid silica sol-gel (home-made [45]) was spun onto the cell (1000 rpm, 10 s) to form a uniform layer of 60–70 nm, and then a PDMS nano-imprint stamp of the wire pattern was applied. This stamp contained three 2.0×2.0 cm^2 nanowire patterns, and an empty 'reference' area to allow comparison of the network-modified areas with a cell fabricated simultaneously on the same Si wafer. After 30 min of curing in ambient conditions, the stamp was removed. The network pattern was then transferred from the solgel into the underlying PMMA by an RIE etch to remove the residual sol-gel layer within the nanowire trenches (150 s, 15 mTorr, 67 W, with 25 sccm CHF_3 and 5 sccm Ar), followed by a 12 min O_2 descum to create trenches in the PMMA.

Thermal evaporation was used to deposit ~2 nm of Ge (0.5 Å/s) and 120 ± 2 nm of Ag (2.0 Å/s) at a base pressure of ~10^{-6} mbar. The Ge functions as a seed layer that controls grain size and improves adhesion. Following evaporation, liftoff was performed by placing the samples vertically into an acetone bath with 10 min megasonication. The nanowire-coated samples were rinsed in isopropanol and dried with N_2. Metallization was completed by evaporating Ag fingers onto the nanowire grid through a laser-cut shadow mask (500 nm, 5–8 Å/s).

Finally, the thin-ITO semicells were overcoated with 62 nm of SiN_x by low temperature PECVD (175 °C). Coating at this temperature had no measurable effect on the physical stability of the nanowire network. For measurement the four cells were laser cut from the semicell wafer (single completed cell: 2.5×2.5 cm^2), and individually attached to copper plates with Ag paste.

4.2. Optical characterization and modeling

Optical reflection spectra were measured using a supercontinuum laser (Fianium SC400-4) in combination with an integrating sphere (LabSphere, 4″). To prevent damage to the networks from the ps-pulsed illumination the laser output was attenuated using a glass wedge; no additional attenuating or focusing optics were required due to the large (4.0 cm^2) area of the NW networks. Reflected light was collected from the sphere using a multi-mode fiber, and measured with a spectrometer (Acton SpectraPro 2300i) and Si CCD (Princeton Pixis 400). Spectra were normalized to the light reflected by a protected Ag mirror. Cell absorption is reported as 1-reflection.

Optical properties for these cell designs were calculated in 3D from λ_0=300–1110 nm using a commercial implementation of FDTD (Lumerical). Nanowire and layer dimensions were identical to the measured experimental values, with dielectric constants determined using spectroscopic ellipsometry.

4.3. Electrical characterization

To determine the sheet resistance of the Ag NW networks in the absence of underlying ITO and Si, NW networks were fabricated on borosilicate glass wafers. Network dimensions were verified to match the networks applied to the semicells using AFM (for height) and SEM (for width, pitch). A thin conductive Ag strip was evaporated through a shadow mask onto two sides of each 2.0×2.0 cm^2 network. The sheet resistance was then determined using a four-point measurement with microprobes connected to a source meter (Agilent B2902A) to measure the IV response between 0.5 and 1 mV in 0.01 mV increments. The sheet resistance was determined by a linear fit to the data. Sheet resistances for both 80 nm and 22 nm ITO were measured using a four-point probe following deposition on SHJ semicells, where the cell was unilluminated and the depletion region was assumed to behave as an insulator.

The current vs. voltage (IV) response of the solar cells was measured under filtered emission from a Xenon lamp to simulate

AM1.5 G illumination (Newport Oriel Sol2A Class ABA), with the output calibrated using a certified reference cell. The IV response was measured with a four-point measurement using a source meter (Agilent B2902A), with two probes contacting the Cu backing plate and two probes on a bus bar connecting the fingers. The measured voltage range was −1.2 to 1.2 V. A shadow mask was used to define the illuminated area; measurements were taken with both an aperture area of 1.8×1.8 cm^2 and 1.8×2.0 cm^2, with currents normalized by the aperture area to give current density. The mask area did not have an influence on the IV response exceeding the cell-to-cell variation from Table 2.

Competing financial interests

The author A.P. has been issued a related patent on metallic nanowire networks.

Acknowledgements

The authors would like to thank Dr. Marc Verschuuren for helpful discussions and assistance in SCIL stamp preparation. This work is part of the research program of the Foundation for Fundamental Research on Matter (FOM) which is part of The Netherlands Organization for Scientific Research (NWO). It is also funded by NanoNextNL, a nanotechnology program funded by the Dutch Ministry of Economic Affairs and the European Research Counsel.

Appendix A. Supplementary material

Supplementary data associated with this article can be found in the online version at http://dx.doi.org/10.1016/j.nanoen.2016.10.011.

References

[1] D.S. Ginley, C. Bright, Transparent conducting oxides, MRS Bull. 25 (2000) 15–18.
[2] C.G. Granqvist, A. Hultaker, Transparent and conducting ITO films: new developments and applications, Thin Solid Films 411 (2002) 1–5.
[3] Z.C. Holman, A. Descoeudres, L. Barraud, F.Z. Fernandez, J.P. Seif, S. De Wolf, C. Ballif, Current losses at the front of silicon heterojunction solar cells, IEEE J. Photovolt. 2 (2012) 7–15.
[4] D.S. Hecht, L. Hu, G. Irvin, Emerging transparent electrodes based on thin films of carbon nanotubes, graphene, and metallic nanostructures, Adv. Mater. 23 (2011) 1482–1513.
[5] T. Minami, Transparent conducting oxide semiconductors for transparent electrodes, Semicond. Sci. Technol. 20 (2005) S35–S44.
[6] Z. Chen, B. Cotterell, W. Wang, E. Guenther, S.-J. Chua, A mechanical assessment of flexible optoelectronic devices, Thin Solid Films 394 (2001) 202–206.
[7] A. Kumar, C. Zhou, The race to replace tin-doped indium oxide: Which material will win?, ACS Nano 4 (2010) 11–14.
[8] S. De, T.M. Higgins, P.E. Lyons, E.M. Doherty, P.N. Nirmalraj, W.J. Blau, J.J. Boland, J.N. Coleman, Silver nanowire networks as flexible, transparent, conducting films: extremely high DC to optical conductivity ratios, ACS Nano 3 (2009) 1767–1774.
[9] J.A. Fairfield, C. Ritter, A.T. Bellew, E.K. McCarthy, M.S. Ferreira, J.J. Boland, Effective electrode length enhances electrical activation of nanowire networks: experiment and simulation, ACS Nano 8 (2014) 9542–9549.
[10] J.H. Yim, S.-Y. Joe, C. Pang, K.M. Lee, H. Jeong, J.-Y. Park, Y.H. Ahn, J.C. de Mello, S. Lee, Fully solution-processed semitransparent organic solar cells with a silver nanowire cathode and a conducting polymer anode, ACS Nano 8 (2014) 2857–2863.
[11] H. Wu, L. Hu, M.W. Rowell, D. Kong, J.J. Cha, J.R. McDonough, J. Zhu, Y. Yang, M.D. McGehee, Y. Cui, Electrospun metal nanofiber webs as high-performance transparent electrode, Nano Lett. 10 (2010) 4242–4248.
[12] Cambrios: ClearOhm® silver nanowire coating. ⟨http://www.cambrios.com/⟩. (accessed 19.02.15)
[13] M. Huang, Z. Hameiri, H. Gong, W.-C. Wong, A.G. Aberle, T. Mueller, Novel hybrid electrode using transparent conductive oxide and silver nanoparticle mesh for silicon solar cell applications, Energy Procedia 55 (2014) 670–678.
[14] M. Göbelt, R. Keding, S.W. Schmitt, B. Hoffmann, S. Jäckle, M. Latzel, V.V. Radmilović, V.R. Radmilović, E. Spiecker, S. Christiansen, Encapsulation of silver nanowire networks by atomic layer deposition for indium-free transparent electrodes, Nano Energy 16 (2015) 196–206.
[15] P.-C. Hsu, S. Wang, H. Wu, V.K. Narasimhan, D.S. Kong, H.R. Lee, Y. Cui, Performance enhancement of metal nanowire transparent conducting electrodes by mesoscale metal wires, Nat. Commun. 4 (2013) 2522.
[16] H. Wu, D. Kong, Z.C. Ruan, P.-C. Hsu, S. Wang, Z. Yu, T.J. Carney, L. Hu, S. Fan, Y. Cui, A transparent electrode based on a metal nanotrough network, Nat. Nanotechnol. 8 (2013) 421–425.
[17] F. Afshinmanesh, A.G. Curto, K.M. Milaninia, N.F. van Hulst, M.L. Brongersma, Transparent metallic fractal electrodes for semiconductor devices, Nano Lett. 14 (2014) 5068–5074.
[18] J. van de Groep, P. Spinelli, A. Polman, Transparent conducting silver nanowire networks, Nano Lett. 12 (2012) 3138–3144.
[19] J. van de Groep, D. Gupta, M.A. Verschuuren, M.M. Wienk, R.A.J. Janssen, A. Polman, Large-area soft-imprinted nanowire networks as light trapping transparent conductors, Sci. Rep. 5 (2015) 11414.
[20] M.G. Kang, L.J. Guo, Nanoimprinted semitransparent metal electrodes and their application in organic light-emitting diodes, Adv. Mater. 19 (2007) 1391–1396.
[21] M.-G. Kang, M.-S. Kim, J. Kim, L.J. Guo, Organic solar cells using nanoimprinted transparent metal electrodes, Adv. Mater. 20 (2008) 4408–4413.
[22] E. Yablonovitch, T. Gmitter, R.M. Swanson, Y.H. Kwark, A 720 mV open circuit voltage SiO_x:c-Si:SiO_x double heterostructure solar cell, Appl. Phys. Lett. 47 (1985) 1211–1213.
[23] S. De Wolf, A. Descoeudres, Z.C. Holman, C. Ballif, High-efficiency silicon heterojunction solar cells: a review, Green 2 (2012) 7–24.
[24] C.-H.M. Chuang, P.R. Brown, V. Bulovic, M.G. Bawendi, Improved performance and stability in quantum dot solar cells through band alignment engineering, Nat. Mater. 13 (2014) 796–801.
[25] A. Polman, M. Knight, E.C. Garnett, B. Ehrler, W.C. Sinke, Photovoltaic materials: present efficiencies and future challenges, Science 352 (2016) aad4424.
[26] M.A. Green, K. Emery, Y. Hishikawa, W. Warta, E.D. Dunlop, Solar cell efficiency tables (version 45), Prog. Photovolt. 23 (2015) 1–9.
[27] K. Masuko, M. Shigematsu, T. Hashiguchi, D. Fujishima, M. Kai, N. Yoshimura, T. Yamaguchi, Y. Ichihashi, T. Mishima, N. Matsubara, T. Yamanishi, T. Takahama, M. Taguchi, E. Maruyama, S. Okamoto, Achievement of more than 25% conversion efficiency with crystalline silicon heterojunction solar cell, IEEE J. Photovolt. 4 (2014) 1433–1435.
[28] M. Taguchi, A. Yano, S. Tohoda, K. Matsuyama, Y. Nakamura, T. Nishiwaki, K. Fujita, E. Maruyama, 24.7% record efficiency HIT solar cell on thin silicon wafer, IEEE J. Photovolt. 4 (2014) 96–99.
[29] A.R. Burgers, How to design optimal metallization patterns for solar cells, Prog. Photovolt: Res. Appl. 7 (1999) 457–461.
[30] S. Schröer, M. Bivour, J. Schön, M. Hermle and S.W. Glunz, Reduction of absorption losses and efficiency gains by investigating amorphous/cristalline SHJ rear emitter solar cells (2CO.14.6), Proceedings of the 27th European Photovoltaic Solar Energy Conference and Exhibition (EU PVSEC), Frankfurt, Germany, 2012, 759–762.
[31] T.W. Ebbesen, H.J. Lezec, H.F. Ghaemi, T. Thio, P.A. Wolff, Extraordinary optical transmission through sub-wavelength hole arrays, Nature 391 (1998) 667–669.
[32] M.A. Verschuuren, Substrate conformal imprint lithography for nanophotonics (Ph.D. thesis), Utrecht University, 2009.
[33] M.A. Verschuuren, P. Gerlach, H.A. van Sprang, A. Polman, Improved performance of polarization-stable VCSELs by monolithic sub-wavelength gratings produced by soft nano-imprint lithography, Nanotechnology 22 (2011) 505201.
[34] M.D. Abbott, J.E. Cotter, T. Trupke, R.A. Bardos, Investigation of edge recombination effects in silicon solar cell structures using photoluminescence, Appl. Phys. Lett. 88 (2006) 114105.
[35] A.F. Mayadas, M. Shatzkes, Electrical-resistivity model for polycrystalline films: the case of arbitrary reflection at external surfaces, Phys. Rev. B 1 (1970) 1382–1389.
[36] M.V. Kurik, Urbach rule, Phys. Status Solidi A 8 (1971) 9–45.
[37] J.L. Elechiguerra, L. Larios-Lopez, C. Liu, D. Garcia-Gutierrez, A. Camacho-Bragado, M.J. Yacaman, Corrosion at the nanoscale: the case of silver nanowires and nanoparticles, Chem. Mater. 17 (2005) 6042–6052.
[38] S.D. Standridge, G.C. Schatz, J.T. Hupp, Toward plasmonic solar cells: protection of silver nanoparticles via atomic layer deposition of TiO_2, Langmuir 25 (2009) 2596–2600.
[39] H. Im, N.C. Lindquist, A. Lesuffleur, S.-H. Oh, Atomic layer deposition of dielectric overlayers for enhancing the optical properties and chemical stability of plasmonic nanoholes, ACS Nano 4 (2010) 947–954.
[40] H. Eom, J. Lee, A. Pichitpajongkit, M. Amjadi, J.-H. Jeong, E. Lee, J.-Y. Lee, I. Park, Ag@Ni core-shell nanowire network for robust transparent electrodes against oxidation and sulfurization, Small 10 (2014) 4171–4181.
[41] M. Knight, Y. Wu, J. Lassiter, P. Nordlander, N. Halas, Substrates matter: influence of an adjacent dielectric on an individual plasmonic nanoparticle, Nano Lett. 9 (2009) 2188–2192.
[42] P. Spinelli, M.A. Verschuuren, A. Polman, Broadband omnidirectional antireflection coating based on subwavelength surface Mie resonators, Nat. Commun. 3 (2012) 692.
[43] A. Mavrokefalos, S.E. Han, S. Yerci, M.S. Branham, G. Chen, Efficient light trapping in inverted nanopyramid thin crystalline silicon membranes for solar cell applications, Nano Lett. 12 (2012) 2792–2796.
[44] B. Demaurex, S. De Wolf, A. Descoeudres, Z. Charles Holman, C. Ballif, Damage at hydrogenated amorphous/crystalline silicon interfaces by indium tin oxide overlayer sputtering, Appl. Phys. Lett. 101 (2012) 171604.
[45] J. van de Groep, P. Spinelli, A. Polman, Single-step soft-imprinted large-area nanopatterned antireflection coating, Nano Lett. 15 (2015) 4223–4228.

Mark W. Knight received his Ph.D in 2014 from Rice University (USA), earning the Ralph Budd Thesis Prize. Subsequently, he has moved to the FOM Institute AMOLF (Netherlands) for a postdoctoral position developing new methods for controlling the flow of light and electrons at the nanoscale. As a member of the Solardam consortium in Amsterdam, he is also studying how nanostructures can be applied over large areas to solve outstanding challenges in solar photovoltaics.

Jorik van de Groep graduated from Utrecht University (cum laude) in 2011 after studying studied both science and innovation management and physics. His doctoral work was completed at the FOM Institute AMOLF (Netherlands) with a thesis titled, "Resonant Nanophotonic Structures for Photovoltaics"; he received his Ph.D (cum laude) from the University of Amsterdam in 2015. He is now a postdoctoral fellow at Stanford University (USA), working on new approaches for light-to-energy conversion.

Paula C.P. Bronsveld studied Astrophysics at the University of Utrecht, where she also completed her Ph.D. thesis on thin film silicon solar cells. In 2008 she began work at ECN Solar Energy as a researcher in the field of silicon materials. Since 2009 she has been involved in the development of (IBC)-heterojunction devices. Currently, she is active as a project leader/researcher in projects on defect mitigation in n-type Cz wafers and various types of passivating contact solar cells.

Wim C. Sinke (1955) is Manager Program Development at ECN Solar Energy, professor Photovoltaic Energy Conversion at the University of Amsterdam, scientific advisor at the FOM Institute AMOLF and co-chairman of the European Photovoltaic Technology Platform. He is also director of the TKI Urban Energy; the national public-private partnership for energy innovation in the urban environment, including solar energy. In 1999 he received the Royal Dutch/Shell Prize, in 2011 the European Becquerel Prize and in 2015 he was appointed a Knight in the Order of the Netherlands Lion for his contributions to the development and promotion of photovoltaic solar energy.

Albert Polman obtained his Ph.D. from the University of Utrecht in 1989, was post-doctoral researcher at AT & T Bell Laboratories until 1991, and then became group leader at AMOLF, where he also served as director from 2006 to 2013. He is currently head of the program "Light management in new photovoltaic materials" and a professor of photonic materials for photovoltaics at the University of Amsterdam. In 2012 he was awarded, together with Harry Atwater, the ENI Renewable Energy Award for his research on light management in photovoltaic materials. Polman is member of the Royal Netherlands Academy of Arts and Sciences (KNAW), Fellow of the Materials Research Society (MRS), and recipient of an ERC Advanced Investigator Grant (2010), the Physica Prize of the Dutch Physical Society (2014) and the Julius Springer Award for Applied Physics (2014).